J Mater Sci (2007) 42:6854–6861
DOI 10.1007/s10853-006-1327-6

Exploring the relationship between ferrite fraction and morphology and the electromagnetic properties of steel

W. Yin · A. J. Peyton · M. Strangwood · C. L. Davis

Received: 8 March 2006 / Accepted: 28 November 2006 / Published online: 26 April 2007

Abstract The link between the electromagnetic properties of steel and its microstructure is a complex one, depending on both phase fractions and morphology. In this paper, both analytical and three-dimensional finite element (3D FEM) modelling techniques were applied to the prediction of permeability for steel with a given ferrite fraction for random ferrite/austenite distributions. Experimental measurements from a multi-frequency electromagnetic sensor on samples generated by hot isostatic pressing (HIPping) of powder mixtures were used to evaluate the analytical and FEM predictions. Theoretical treatment of the relationship between the sensor output and the effective permeability is also given; in particular, it was found that the zero crossing frequency of the real part of the inductance is approximately linearly related to the permeability for high (> 40%) ferrite percentages. The EM sensor can therefore be used to identify the samples across the full range (0–100%) of ferrite percentages using both the zero crossing frequency (> 40%) and trans-impedance (0–40%). The effect of banded (non-random) microstructures on sensor output and the prediction of the upper and lower bounds of permeability are also discussed.

W. Yin · A. J. Peyton
School of Electrical and Electronic Engineering, University of Manchester, Manchester M60 1QD, UK

M. Strangwood · C. L. Davis (✉)
Department of Metallurgy and Materials, University of Birmingham, Edgbaston, Birmingham B15 2TT, UK
e-mail: c.l.davis@bham.ac.uk

Introduction

The production of strip steel with dual or multi-phase microstructures by direct rolling and cooling requires accurate process control. Electromagnetic (EM) techniques have the advantage of being non-contact, robust and offer the potential for direct microstructure characterisation. However, the key to the successful application of EM techniques is to decode the complex relation in the transduction chain (Fig. 1) from microstructure to the EM properties, and to the sensor output across the whole range of ferrite fraction. The main EM property that affects the sensor output is permeability as the range of conductivity variation (for instance, 5.75–6.13MSm^{-1} for AISI 1000 Series steel) is much less than that of the permeability (1 to $\gg$ 100 relative permeability values [1]. Previously interrupted cooling experiments, coupled with Maxwell 2D FEM simulations, on a medium carbon (0.45 wt% C) steel examined the relationship between sensor trans-impedance and ferrite percentage, up to 28% ferrite, during transformation from austenite to ferrite on cooling [2, 3]. The relationship between the output of a multi-frequency electromagnetic sensor and the ferrite percentage for randomly oriented microstructures was explored with samples with the full range (0–100%) of ferrite fractions [4].

So far, the strategy has been to link the microstructure directly with sensor output. Although the EM sensor output has proved to be a valid indicator of microstructure, it depends on sensor geometrical factors as well. Therefore, conclusions drawn from one sensor do not necessarily apply to another. In this paper, an alternative approach is proposed: the full transduction chain is considered in two steps. The first step is to link the microstructure to the fundamental EM properties (mainly permeability), and the second step is to link the fundamental EM properties to the

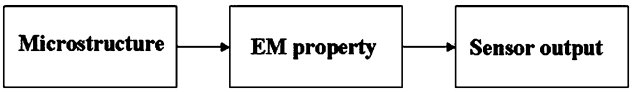

Fig. 1 Illustration of the transduction chain

sensor output. This approach enables us to gain full physical insight into the transduction chain and set up general models independent of sensor geometry.

Theory

The link between microstructure and steel permeability

The problem of predicting an effective electrical or magnetic property in a two-phase (ferrite/austenite) composite medium, for a given ferrite fraction, can be dealt with by effective medium theory. Effective medium theory deals with the question of predicting effective conductivity/permittivity/permeability values for mixtures having two or more phases with contrasting properties. The principle of the effective medium theory is that the electrical/magnetic potential due to the mixture placed in the external electrical/magnetic field is equal to the potential caused by a geometrically identical object having an effective conductivity/permeability/permittivity. Although cases for predicting effective permeability are rare, many formulae have been developed for predicting effective conductivity and permittivity [5–8].

Maxwell's equation is the earliest work on the prediction of effective conductivity of a cell suspension in a dilute solution [5].

$$\sigma_{\text{effective}} = \sigma_e + \frac{f}{\frac{1}{\sigma_i - \sigma_e} + \frac{1-f}{3\sigma_e}} \tag{1}$$

where $\sigma_{\text{effective}}$ is the effective conductivity, and σ_e and σ_i are the solution conductivity and conductivity of particles in suspension respectively. f is the particle volume faction.

Bruggeman extended Maxwell's equation to concentrated suspensions by a mathematical procedure [6, 7] and obtained the result known as Bruggeman's formula.

$$\frac{\sigma_{\text{effective}} - \sigma_i}{\sigma_e - \sigma_i}\left(\frac{\sigma_e}{\sigma_{\text{effective}}}\right)^{1/3} = 1 - f \tag{2}$$

The Maxwell and Bruggeman equations are not valid for the entire range of particle volume fractions (f of 0–1) with the extent of the valid range being dependent on the difference in conductivities between the particles and solution. For weakly contrasting media (i.e. similar conductivities), the upper limit of f for which Eq. (2) is valid is expected to be higher than for strongly contrasting media; Pavlin [8] reported a good agreement between the analytical equations and an FEM model for volume fractions up to 0.7 for media with a difference in conductivity of a factor of 10. For the strongly contrasting media in this study (permeability values differ by a factor of 100), the valid range of f is expected to be much lower [9].

Power-law models are popular for predicting effective permittivity. They give the effective permittivity of the mixture as

$$\varepsilon^{\beta}_{\text{effective}} = (1-f)\varepsilon^{\beta}_{e} + f\varepsilon^{\beta}_{i} \tag{3}$$

where β is a dimensionless parameter. Known examples are the Birchak formula (β = 1/2) [10] and the Looyenga formula (β = 1/3) [11].

The applicability of these formulae to the case of predicting effective permeability will be evaluated in the following sections.

The link between permeability and sensor output

In previous studies, it has been shown that the ferrite fraction has an approximately linear relationship with the zero-crossing frequency and has a strongly non-linear relationship with the inductance at low frequency (for ferrite percentages above 40%), determined from experimental tests using a multi-frequency EM sensor [4]. Therefore, for the industrial application of monitoring ferrite percentage in multi-phase strip steel production before coiling after hot strip rolling, where the ferrite percentages of interest are typically 70–90%, the zero-crossing frequency has to be determined.

The zero crossing frequency can be explained qualitatively as follows. The magnetic field produced by a multi-frequency sensor acts on a ferromagnetic target in two ways. First it tends to magnetize the metal, which increases the coil's inductance. Second, the ac magnetic field also induces eddy currents in the metal, which tend to oppose the driving current and reduce the coil's inductance. At lower frequencies, magnetization dominates and inductance is positive. As the frequency is increased eddy currents become more dominant and the inductance decreases, at some point becoming negative, and eventually approaching a constant value at high frequencies. When the two effects are in balance there is a zero crossing point frequency (i.e. the frequency at which the inductance is zero).

To gain a quantitative understanding of the link between permeability and the zero-crossing frequency, Dodd and Deeds' complete analytical solution for sensor output due to the presence of a thick magnetic sample is used [12].

The formulae of Dodd and Deeds are:

$$L(\omega) = K \int_0^{\infty} \frac{P^2(\alpha)}{\alpha^6} A(\alpha)\phi(\alpha)d\alpha \tag{4}$$

where

$$\phi(\alpha) = \frac{(\mu\alpha - \alpha_1)}{(\mu\alpha + \alpha_1)} \tag{5}$$

$$\alpha_1 = \sqrt{\alpha^2 + j\omega\sigma\mu_0\mu} \tag{6}$$

$$K = \frac{\pi\mu_0 N^2}{(l_1 - l_2)^2 (r_1 - r_2)^2} \tag{7}$$

$$P(\alpha) = \int_{\alpha r_1}^{\alpha r_2} xJ_1(x)dx \tag{8}$$

$$A(\alpha) = (e^{-\alpha l_1} - e^{-\alpha l_2})^2 \tag{9}$$

where L denotes inductance and j is defined as $(-1)^{0.5}$. μ_0 denotes the permeability of free space and μ denotes the relative permeability of the sample. N denotes the number of turns in the coil; r_1 and r_2 denote the inner and outer radii of the coil, while l_1 and l_2 denote the height of the bottom and top of the coil; and c denotes the thickness of the plate. σ is the conductivity of the sample. ω is the angular frequency of alternating current signal to excite the sensor. α is a spatial frequency variable; K is a pre-factor and $J_1(x)$ is a first-order Bessel function.

Two approximations can be used to derive the zero-crossing frequency in the case of $\mu \gg 1$. The first approximation originates from the fact that $\varphi(\alpha)$ varies slowly with α compared to the rest of the integrand, which reaches its maximum at a characteristic spatial frequency α_0. α_0 is defined to be one over the smallest dimension of the coil. The approximation is to evaluate $\varphi(\alpha)$ at α_0 and take it outside of the integral.

$$\Delta L(\omega) = \phi(\alpha_0)\Delta L_0 \tag{10}$$

$$\phi(\alpha_0) = \frac{\mu\alpha_0 - \sqrt{(\alpha_0^2 + j\mu\mu_0\sigma\omega)}}{\mu\alpha_0 + \sqrt{(\alpha_0^2 + j\mu\mu_0\sigma\omega)}} = \frac{1 - \sqrt{1/\mu^2 + j\mu_0\omega\sigma/\mu\alpha_0^2}}{1 + \sqrt{1/\mu^2 + j\mu_0\omega\sigma/\mu\alpha_0^2}} \tag{11}$$

The second approximation is to neglect the term $1/\mu^2$ in Eq. (11). This condition is met when the skin depth is much smaller than the coil dimension. Based on this assumption and considering Eq. (11), Eq. (10) becomes

$$\Delta L(\omega) = \Delta L_0 \frac{1 - \sqrt{j\mu_0\omega\sigma/\mu\alpha_0^2}}{1 + \sqrt{j\mu_0\omega\sigma/\mu\alpha_0^2}} \tag{12}$$

For the real inductance to equal zero, we have

$$\omega_0 = \frac{\mu\alpha_0^2}{\mu_0\sigma}. \tag{13}$$

Equation (13) indicates that the zero-crossing frequency (ω_0) is linearly proportional to permeability. This relationship will be used to evaluate the validity of permeability predictions by FEM and analytical techniques. This relationship holds for many practical coil geometries as formulations for the inductance of most coils can be simplified to Eq. (10) [13], although the coefficient α_0 may vary. The range of conductivity values was found to be small (≈5%) using measurements from a standard four terminal method on the HIPped samples with a range of ferrite percentages from 0 to 100%. Therefore the variation in conductivity is expected to have a very small effect on the zero crossing frequency compared to the permeability and has been ignored in the subsequent analysis.

Modelling

FEM modelling and the electrostatic and magnetostatic analogy

Previously, 2D and 3D eddy current simulations [2, 3, 4] were performed to predict the multi-frequency EM sensor output. In those simulations, the diffusion equation was solved and a specific sensor geometry was used. In this paper, the strategy is to seek a sensor geometry that can be easily used to derive the effective permeability.

To derive the effective permeability from the sensor output accurately, regular and simple structures are preferred. The toroidal structure (Fig. 2) is a good candidate, because there is a simple analytical solution that links the sensor output to the permeability [14].

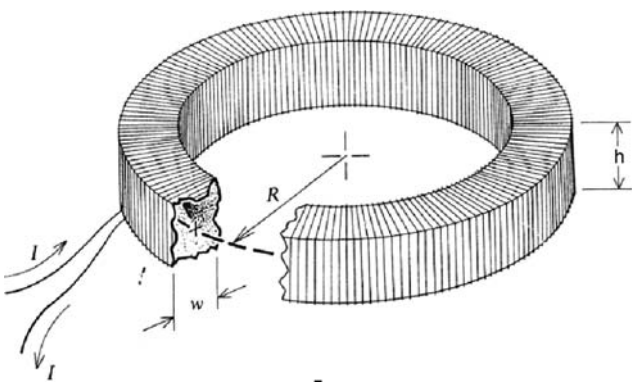

Fig. 2 The geometry of the toroidal coil [14]

$$\mu_r = \frac{L2\pi}{N^2\mu_0 h \ln\left[\frac{2R+w}{2R-w}\right]} \quad (14)$$

where μ_r and μ_0 stand for the relative permeability and free space permeability respectively. L is the inductance and N is the number of turns. The other geometrical parameters are shown in Fig. 2.

However, it is not straightforward to thread coils around the toroidal structure and magnetic linkage needs to be minimised. In this paper, it is proposed that by utilising the analogy between electrostatics and magnetostatics, the simulation can be simplified to a parallel plate capacitor where the effective permittivity is sought. Table 1 lists the corresponding quantities in electrostatics and magnetostatics respectively. The analogy is guaranteed since the governing equation for both cases is the LaPlace equation for electrical potential and magnetic scalar potential.

FEMs of a parallel plate capacitance sensor were constructed to predict the effective permittivity of the mixtures, with the phases of the mixtures being set to have contrasting permittivities, which are equivalent to permeability in magnetic cases. The mixture is considered to be comprised of isolated spheres of one phase distributed randomly within the other phase. Overlapping spheres were coalesced by using a unite function in the Maxwell software (Ansoft Corporation) [15].

The effective permittivity of the medium in a parallel capacitance sensor is

$$\varepsilon_r = \frac{Cd}{\varepsilon_0 A} \quad (15)$$

where C denotes the capacitance value. A and d denote the area and the separation between the two plates respectively. ε_r and ε_0 stand for the relative permittivity and free space permittivity respectively.

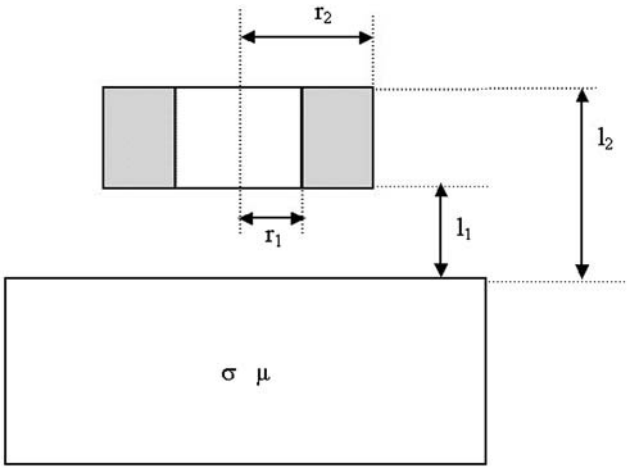

Fig. 3 Schematic diagram of the geometry of the coil and the steel sample

Table 1 Analogy between electrostatics and magnetostatics

Electrostatics	Magnetostatics
Permittivity	Permeability
Relative permittivity	Relative permeability
Electrical potential	Magnetic scalar potential
Electrical flux	Magnetic flux
Capacitance	Inductance

Figure 4 shows the FEM simulations for 5, 10, and 20% of high permittivity materials.

Comparison between the permeability predictions from the FEM model and analytical formulas

Figure 5 shows the predicted permeability from the analytical formulae compared to the output of the FEM model versus ferrite percentage for random microstructures. The ferromagnetic regions were assigned a relative permeability of 200 and the paramagnetic regions a value of 1 [16]. As can be seen in Fig. 5, the closest matches with the FEM prediction are the power-law models, i.e. Birchak and Looyenga. The difference between the Birchak and Looyenga models is their power coefficients, which determine the shape of the curve. It is found that the upper and lower bounds (see Conclusions) can be obtained by evaluating the power-law model at $\beta = -1$ and $\beta = 1$.

The poor fit between the Maxwell and Bruggeman equations and the FEM model over the entire range of ferrite percentage values may be related to the fact that these equations were derived for mixtures of different conductivities and their application for mixtures of different permeabilities may be limited. This is due to the analogy between conductivity and permeability being inappropriate for some specific materials cases. For instance with the conduction case, the conductivity of one phase can be zero, but this has no practical analogy in the magnetostatic context, where the lowest (relative) permeability and permittivity can only be approximately 1. The analogy between the magnetostatic and electrostatic cases (i.e. pemittivity and permeability) on the other hand is exact, which may help to explain the better fit for the Birchak and Looyenga models.

Experimental validation of the models

Experimental details of HIPped samples

In this work, model microstructures of known ferrite, from 0 to 100%, and austenite percentages at room temperature,

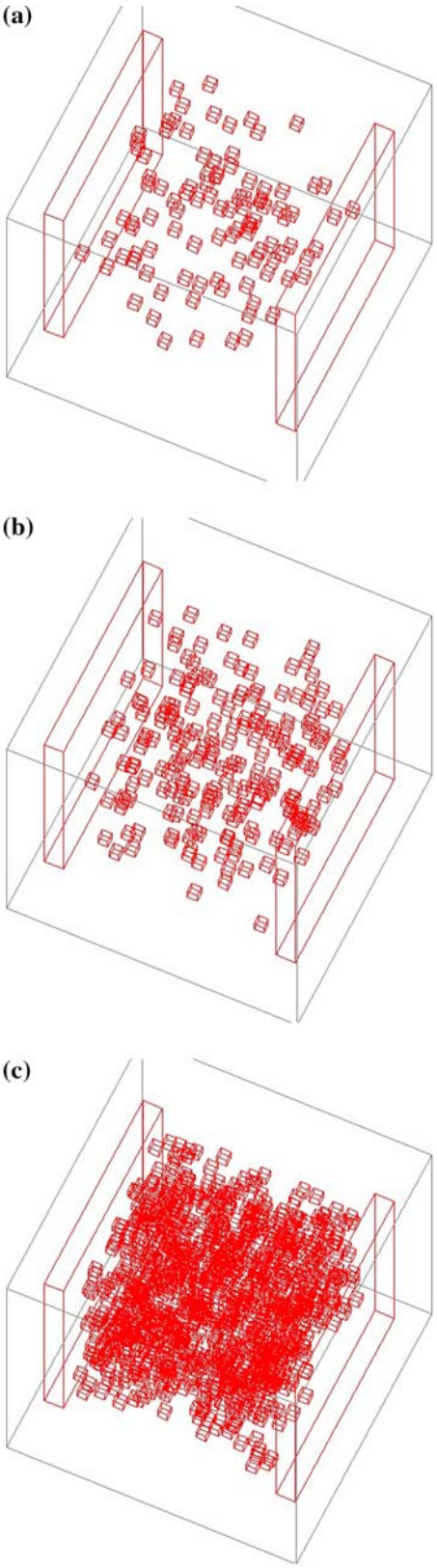

Fig. 4 FEM simulations with varying percentages of high permittivity phase

were generated by a powder/hot isostatic pressing (HIPping) route using 112 μm diameter mean particle size austenitic stainless steel (316L) powder, which is paramagnetic, and 65 μm diameter mean particle size ferritic (434L) stainless steel, which is ferromagnetic at room temperature. Conditions for HIPping were chosen as 1000 °C at 150 MPa for 120 min to limit diffusion between the two compositions and therefore minimise the amount of intermediate phases produced [17]. The samples were machined to remove the austenitic stainless steel can used to contain the powder, into a disc (43 mm diameter, 10 mm thick) for EM measurements.

Sensor set-up description

An air-cored coil as shown in Fig. 3, was used. The coil parameters are $r_1 = 20$ mm, $r_2 = 20.1$ mm, $h = 2$ mm, and $N = 10$. The inductance measurements for all samples were taken using an impedance analyser (SL1260) at frequencies from 100 Hz to 1 MHz.

Sensor output for random microstructures

The inductance measurements at frequencies from 100 Hz to 1 MHz are plotted in Fig. 6. Consistent with the discussion in section ''the link between permeability and sensor output'', the coil inductance at low frequencies is positive, and as the frequency increases, it decreases, crosses zero and becomes negative. This is due to the competing effects of magnetisation and eddy currents.

As shown in Fig. 7, the ferrite percentage from approximately 40–100% can be easily identified through the zero crossing frequency using the multi-frequency inductance spectroscopic method as an approximately linear relationship exists between the zero crossing frequency and ferrite percentage. For the low frequency inductance value an approximately linear relationship with ferrite percentage is seen for low ferrite percentages (approximately 0–40%), this is due to the fact that the low frequency inductance is non-linearly related to permeability and reaches saturation when the ferrite percent (and hence effective permeability) forms connected ferromagnetic pathways through the material; while the zero crossing frequency is sensitive to larger effective permeabilities (higher ferrite percentages) and does not have the problem of saturation.

Equation (13) indicates that the zero crossing frequency is proportional to the effective relative permeability when it is much greater than 1. Combined with the fact that the FEM and power-law models show that the effective relative permeability is expected to be proportional to ferrite percentage above ≈35%, therefore one would expect the

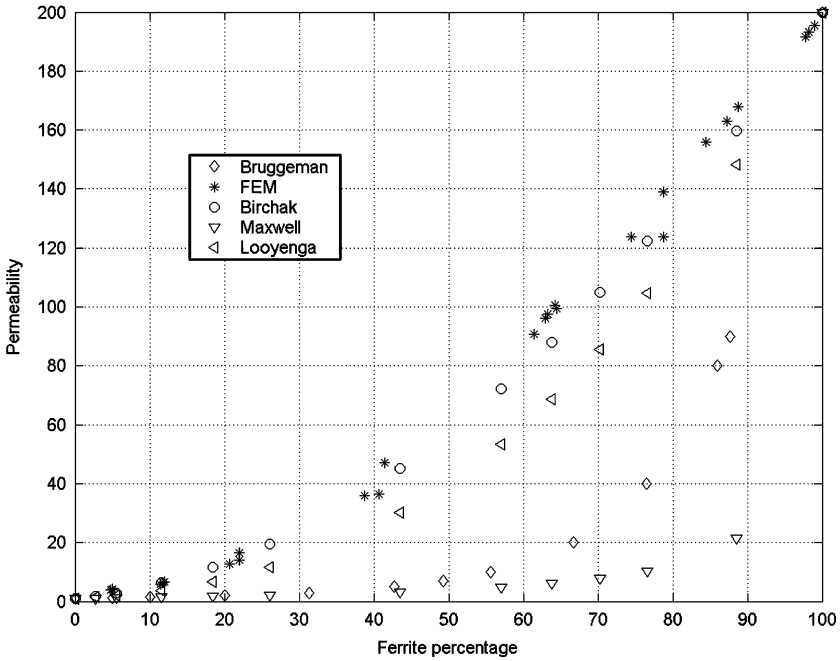

Fig. 5 Predicted permeability from the FEM model and the analytical formulae

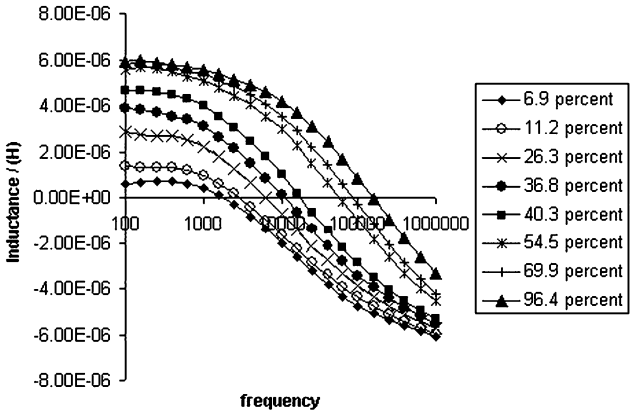

Fig. 6 The measured inductance curves for the HIPped samples, from which the zero-crossing frequency was identified

zero crossing frequency to be proportional to the ferrite percentage also above ≈35% ferrite percentage, which is supported by Fig. 7b where the linear relationship appears to be valid above a ferrite percentage of 40%. For ferrite percentages below around 35%, the assumption for Eq. (13) to be valid does not hold (i.e. the relative permeability is not $\gg 1$), and therefore the linear relationship does not hold. This result is extremely useful for the industrial processing of dual and multi-phase strip steels where the ferrite percentages of interest (measured after hot rolling and water cooling before hot coiling) are typically in the range 70–90%.

The significance of this result is that a simple analytical model can be used to predict the effective permeability for random microstructures of ferrite and austenite with good accuracy, which means that the ferrite percentage can be easily deduced from the sensor output (e.g. zero-crossing frequency) using Eq. (13), if the coefficient α_0 is calibrated using numerical or experimental results for a given sensor geometry.

For more complex, non-random microstructures, however, a more powerful and computationally intensive finite element method (FEM) is needed.

Sensor output for banded, i.e. non-random microstructures

So far, the case for randomly distributed microstructures has been considered. For non-randomly distributed microstructures, such as banded ones, the effective permeability can vary widely for a given ferrite percentage. Models that can describe non-randomly distributed microstructures have yet to be found. However, the upper and low bounds for permeability based on extremes of ferrite morphology (aligned parallel or perpendicular to the magnetic flux) can be calculated. Using formulae based on the capacitance of a parallel plate sensor, we have

$$\mu_{\text{effective,max}} = f\mu_i + (1-f)\mu_e \tag{16}$$

$$\mu_{\text{effective,min}} = \frac{\mu_i \mu_e}{f\mu_e + (1-f)\mu_i} \tag{17}$$

It is found that they can be obtained by evaluating the power-law model at $\beta = -1$ and $\beta = 1$. Figure 8 plots the upper and lower bounds based on Eqs. (16) and (17), and the FEM and analytical solutions for the random microstructures, which all lie within the bounds as would be expected.

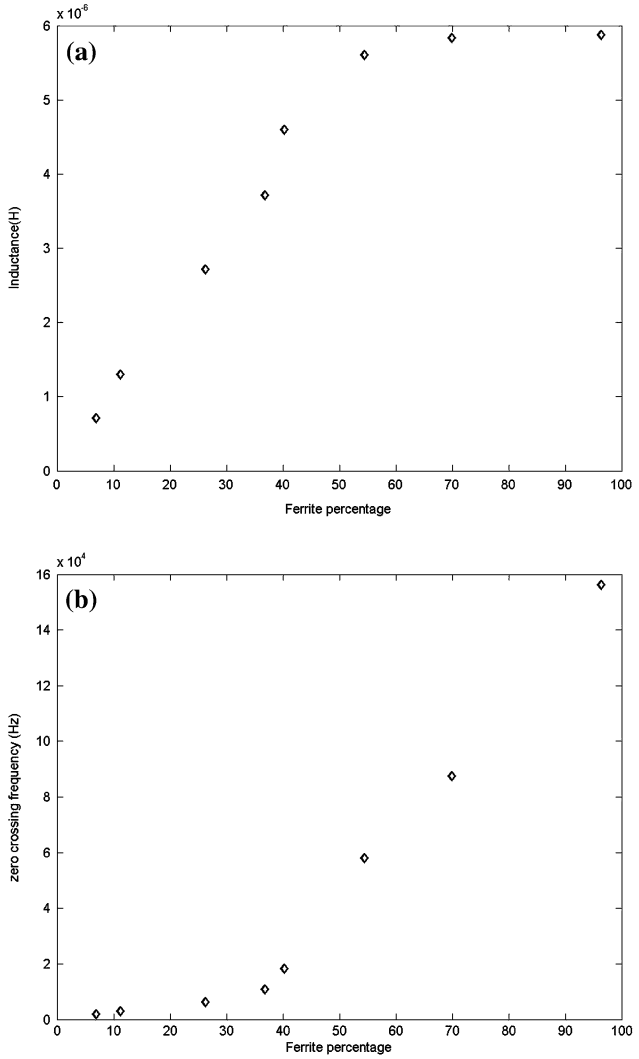

Fig. 7 (**a**) The relationship between low frequency inductance and ferrite percentage and (**b**) the relationship between zero crossing frequency and ferrite percentage

To detect anisotropy in a microstructure using EM techniques, EM sensors that produce directionally preferable flux are needed, one example being U-shaped ferrite-cored sensors. Measurement results were made along the rolling direction and perpendicular to the rolling direction for an extruded billet sample produced from HIPped powder. The microstructure of the extruded billet sample, Fig. 9a, shows an elongated grain structure compared to the as-HIPped sample, Fig. 9b. The sensor output, in terms of the real inductance versus frequency is given in Fig. 10. It can be seen that the zero-crossing frequency is only slightly affected by the orientation of the sample (i.e. the anisotropy in microstructure) giving values of 4.5 and 5.1×10^4 Hz, which can be equated to a ferrite percent (for a random microstructure) of approximately 49.8% to 52.1% from Fig. 7(b) – the measured area percent of ferrite in the sample is 50%. This corresponds to a variation of

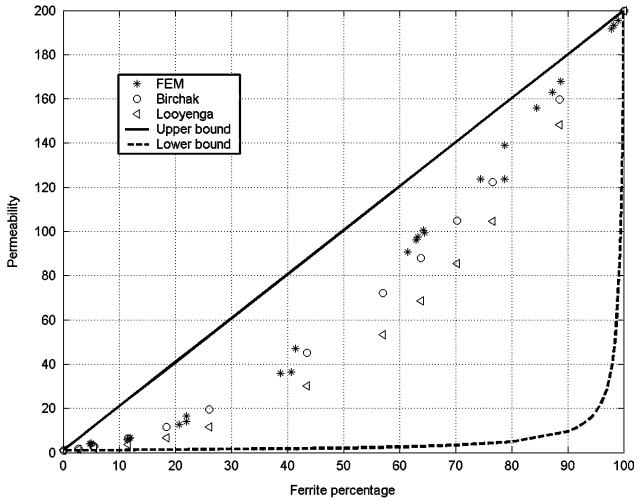

Fig. 8 The upper and lower bounds for the effective permeability of non-random microstructures

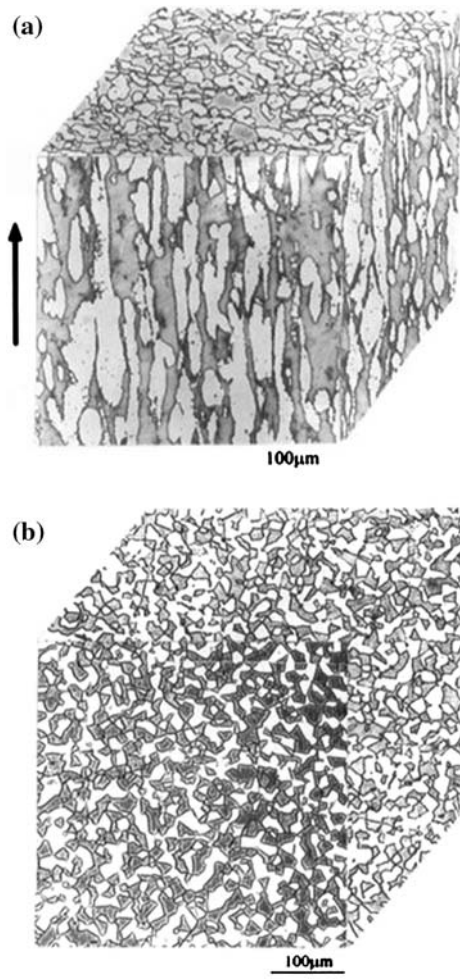

Fig. 9 Micrographs of (**a**) the extruded billet sample showing the preferred magnetic path along the rolling direction (arrowed) and (**b**) the as-received HIPped sample showing a random microstructure

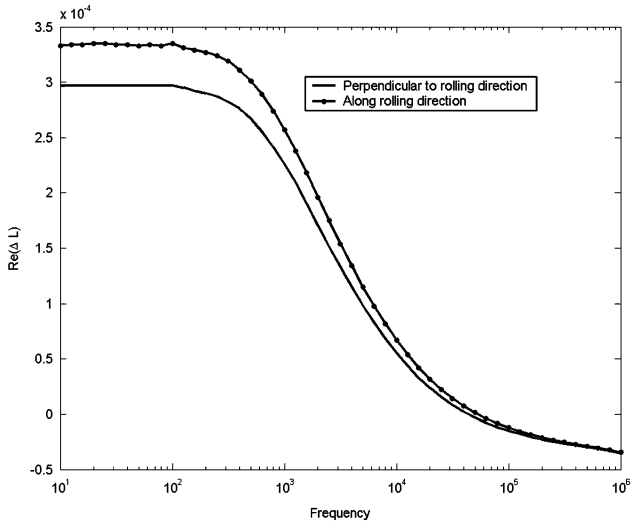

Fig. 10 Measurement results along the rolling direction and perpendicular to the rolling direction for an extruded billet sample

2.3% in ferrite percentage, which is within the expected range from material inhomogeneity due to powder processing. Considering that this variation is likely to be larger for lower ferrite percentages (sensor output is less linear with and more sensitive to frequency), it is estimated that the accuracy over the full range is likely to be within 5%. Therefore the extent of banding will not be accurately determined by zero crossing frequency measurements.

However the real inductance at low frequencies (< 100 Hz) is significantly affected by the anisotropy in microstructure, where along the rolling direction the magnetic reluctance is smaller as the ferromagnetic phase (ferrite) is elongated in this orientation and flux is easier to pass and therefore the output of the sensor is larger. Therefore the low frequency inductance can be used to determine the degree of anisotropy (i.e. how banded) of the microstructure whereas the zero-crossing frequency can be used to determine the ferrite fraction (for the samples examined).

The next stage of the work is to develop FEM simulations to account for non-random aligned microstructures. Preliminary results indicate that the EM sensor(s) with directionally preferable magnetic path can give a measure of anisotropy (banding, which is the common microstructural morphology seen in rolled strip and plate steels) through the low frequency real inductance but that the ferrite percentage can still be estimated from the zero-crossing frequency, which seems to be less affected by microstructural anisotropy, as the two curves tend to converge at high frequencies.

Conclusions

This paper has explored the link between the electromagnetic properties of steel and its microstructure. For random ferrite/austenite distributions, it is believed that Birchak formula gives the best prediction of effective permeability compared to both 3D FEM analysis and other analytical equations. The zero-crossing frequency has been related to the effective permeability of the randomly orientated mixed ferrite and austenite samples. It has been shown that the zero-crossing point frequency can be used to measure the ferrite percentage for samples containing greater than about 40% ferrite, whereas the inductance can be used for samples with less than 40% ferrite. It is possible to distinguish the rolling direction of banded microstructures and give predicted permeability bounds for such microstructures. Further research, possibly using multi-frequency sensors with different sensing directions to simultaneously determine the morphology and ferrite fraction is needed.

Acknowledgements The authors wish to express their gratitude to EPSRC for their financial support and Corus (UK) Ltd. for financial support and extremely valuable technical input, the Engineering Department at Manchester University for the electronic test instrumentation and the Department of Metallurgy and Materials at the University of Birmingham for the provision of facilities.

References

1. http://www.matweb.com as on 15.11.06
2. Davis CL, Papaelias MP, Strangwood M, Peyton AJ (2002) Ironmak Steelmak 29(6):469
3. Papaelias MP, Strangwood M, Peyton AJ, Davis CL (2004) Metallur Mater Trans A 35A:965
4. Haldane RJ, Yin W, Strangwood M, Peyton AJ, Davis CL (2006) Scripta Mat 54(10):1761
5. Maxwell JC (1873) In: Treatise on electricity and magnetism. Oxford Univ. Press, UK
6. Matijevic E (1971) Surface and colloid science, in dielectric properties of disperse systems, vol 3. Wiley-Interscience, New York, pp 83
7. Sherman P (1968) Emulsion science, in electrical properties of emulsions. London, U.K., Academic, pp 353
8. Pavlin M, Slivnik T, Miklavcic D (2002) IEEE Trans Bio Med Eng 49:77
9. Pellegrini YP (2000) Phys Rev B 61:9365
10. Birchak JR, Gardner LG, Hipp JW, Victor JM (1974) In: Proceedings of the IEEE 62:93
11. Looyenga H (1965) Physica 21:410
12. Dodd CV, Deeds WE (1968) J Appl Phys 39:2829
13. Yin W, Binns R, Davis CL, Peyton AJ, Dickinson SJ (2002) In: Proceedings of the IEEE instrumentation and measurement technology Conference, Ottawa, Canada, May 2005, ISBN 0-7803-8880-1
14. Lorrain P, Corson D (1988) Electromagnetic fields and waves. Freeman, New York, pp 347
15. Maxwell user manual, Ansoft Corporation, 2001
16. Stainless Steels (1994) In: Davis JR (ed) ASM speciality handbook, pub. ASM International, ISBN 0-87170-503-6
17. Marcu Puscas T, Molinari A, Kazior J, Pieczonka T, Nykiel M (2001) Powder Metallur 44(1):48